THE JOURNAL OF PHYSICAL CHEMISTRY C

ARTICLE

pubs.acs.org/JPCC

The State of Asymmetric Nitride Clusters in Endohedral Fullerenes as Studied by ^{14}N NMR Spectroscopy: Experiment and Theory

Alexey A. Popov,*[,†,‡] Sandra Schiemenz,[†] Stanislav M. Avdoshenko,[§] Shangfeng Yang,[†,#] Gianaurelio Cuniberti,[§,∥] and Lothar Dunsch*[,†]

[†]Department of Electrochemistry and Conducting Polymers, Leibniz Institute of Solid State and Materials Research, Dresden, D-01069 Dresden, Germany

[‡]Chemistry Department, Moscow State University, 119992 Moscow, Russia

[§]Institute for Materials Science and Max Bergmann Center of Biomaterials, Dresden University of Technology, D-01062 Dresden, Germany

[∥]Division of IT Convergence Engineering and National Center for Nanomaterials Technology, POSTECH, Pohang 790-784, Republic of Korea

ABSTRACT: While the role of asymmetric nitride clusters on the cage size and symmetry in fullerene-based structures is already well-known, the role of the asymmetric arrangement of metals in nitride clusters on the nitrogen is studied in detail in this work. It is discovered that asymmetric mixed-metal nitride clusters give sufficiently narrow ^{14}N NMR signals to make NMR the method of choice to characterize the endohedral cluster from the inside. In the series of mixed-metal nitride clusterfullerenes $Lu_xSc_{3-x}N@C_{80}$ and $Lu_xY_{3-x}N@C_{80}$ (x = 0−3) the $\delta(^{14}N)$ values are found to be linear functions of x showing that ^{14}N chemical shifts are additive values with specific increment for each kind of metal atoms. Density functional theory calculations are performed to interpret the experimentally measured spectra. To reveal the main factors affecting ^{14}N chemical shifts in nitride clusterfullerenes, shielding tensor components are analyzed in terms of Ramsey theory both in localized and canonical molecular orbitals. ^{14}N chemical shifts in $M_3N@C_{80}$ and related systems are shown to be determined solely by nitrogen-localized orbitals and in particular by the $p_{x,y,z}$ atomic orbitals of nitrogen. As a result, the peculiarities of the nitrogen shielding in nitride clusterfullerenes can be interpreted by the simple analysis of the nitrogen-projected density of states and its variation in different chemical environments.

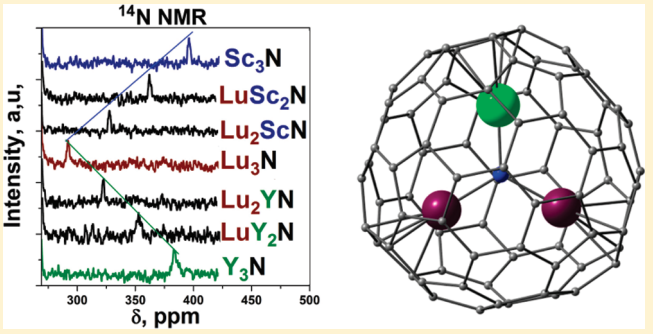

INTRODUCTION

Among the endohedral metallofullerenes (EMFs) encapsulating one or more metal atoms or a cluster in their inner space, the nitride clusterfullerenes exhibit the largest variety of structures both for the cage and the cluster.[1,2] With the formal charge distribution of $(M_3N)^{6+}@C_{2n}^{6-}$, such EMFs have a large extent of the electron transfer between the cluster and the carbon cage making the electronic state of such fullerenes very special and stabilizing carbon cages, which are not sufficiently stable in their neutral state.

From the structural point of view, the three "shells" constituting the key elements of nitride clusterfullerenes can be distinguished: the outer carbon cage, the central nitrogen atom, and three metal atoms in between. In the spectroscopic studies of EMFs, the carbon cages have by far the highest impact. For instance, absorption spectra are dominated by $\pi \rightarrow \pi^*$ excitations of the fullerene;[1,3] likewise, vibrational spectra are dominated by the carbon cage vibrations (except for the low-frequency range, in which metal-based vibrations can be seen).[4] Electrochemical properties of nitride clusterfullerenes are mostly determined by their carbon cages[2,5] (however, there is a recent review[6] on special cases of endohedral electrochemistry). ^{13}C NMR has been a standard tool in the studies of fullerenes and EMFs for two decades, and even some paramagnetic lanthanides can be successfully studied by this method.[7−12] Importantly, the carbon cage in EMF is by no means an "innocent ligand", and spectroscopic response is to a large extent determined by the interaction with the endohedral cluster.[13] We have recently shown that even subtle changes in the local pyramidalization angles of the metal-bonded carbon atoms induced by the increase of the cluster size in the series of $Lu_xSc_{3-x}N@C_{80}$ and $Lu_xY_{3-x}N@C_{80}$ (x = 0−3) EMFs can be revealed with the use of ^{13}C NMR spectroscopy.[14]

Received: May 9, 2011
Revised: June 30, 2011
Published: July 01, 2011

Vast majority of spectroscopic studies focusing on the metal atoms is limited to high-energy spectroscopy, which reveals that changes to the core electron levels of endohedral metal atoms in dependence on their bonding states.[15−19] For paramagnetic states of EMFs (either in the pristine form for intrinsically paramagnetic EMFs or those generated electrochemically[6]), electron spin resonance (ESR) spectroscopy was found to be a useful tool, especially for Sc-,[20−25] Y-,[26−29] and La-based EMFs[26,30−34] since hyperfine structure due to interaction of these metals with the unpaired spin is readily available in clockwise X-band ESR spectroscopy. Likewise, these elements also allow for metal-based NMR spectroscopic studies, which have been successfully employed in the studies of the structure and dynamics of endohedral clusters.[12,35−41]

Direct observations of the spectroscopic response of the central nitrogen atoms in nitride clusterfullerene are rather rare. To our knowledge, only one work reports on the 1s (N) photoemission study of nitrogen in $Sc_3N@C_{80}$;[15] we are not aware of such studies for other EMFs. Hyperfine structure due to nitrogen has been observed only in the ESR spectrum of the anion-radical of pyrrolidine adduct of $Y_3N@C_{80}$;[28] N-based splitting could be found neither for the charged states of $Sc_3N@C_{68}$ nor for those of $Sc_3N@C_{80}$ and its derivatives. Till recently, IR spectroscopy has been the most informative technique in the studies of the central nitrogen atom state in nitride clusterfullerenes since high intensity of the antisymmetric metal−nitrogen stretching mode facilitated its observation in the experimental spectra.[42−48] Theoretical studies have shown that in this mode heavy metal atoms do not move, while the nitrogen oscillates in the plane of the M_3N cluster.[4,42] We have found that the frequency of this mode is dependent on the cluster pyramidalization state;[44] besides a correlation between the frequency and the metal−bond length was established.[4,45] Thus, this mode is found to be a convenient marker of the metal−nitrogen bonding situation. Although nitrogen has nonzero nuclear spin, the use of NMR spectroscopy is mostly focused on the ^{15}N isotope, since it is believed that the quadrupolar moment of ^{14}N nuclei severely broadens the signal and makes ^{14}N NMR studies hardly useful. On the other hand, the low natural abundance of ^{15}N isotope precludes the broad use of ^{15}N NMR spectroscopy in routine studies of nitrogen-containing fullerenes. However, it has been shown recently by Dorn et al. that the rarely applied ^{14}N NMR spectroscopy is a useful tool to characterize nitride cluster fullerenes.[49] These authors have studied ^{14}N NMR spectra of $Sc_3N@C_{80}$, $Y_3N@C_{80}$, and $Lu_3N@C_{80}$ and have shown that these EMFs exhibit surprisingly narrow ^{14}NNMR peaks. This fact was attributed to the symmetric environment of the nitrogen atoms provided by homometallic clusters. In this work we use ^{14}N NMR spectroscopy to extend our understanding of the nitrogen states in the mixed-metal nitride clusterfullerenes $Lu_xSc_{3-x}N@C_{80}$ and $Lu_xY_{3-x}N@C_{80}$ ($x = 0−3$) and show that equally narrow ^{14}N signal can be observed for the mixed-metal clusters. Extended theoretical study in the framework of Ramsey theory[50] is performed to reveal the factors determining the magnitude of ^{14}N chemical shifts in nitride clusterfullerenes.

RESULTS AND DISCUSSION

Experimental ^{14}N NMR Spectra. Figure 1 shows ^{14}N NMR spectra of $Lu_xSc_{3-x}N@C_{80}$ and $Lu_xY_{3-x}N@C_{80}$ ($x = 0−3$) nitride clusterfullerenes measured in CS_2 solution at room temperature. For each compound, either with homometallic or

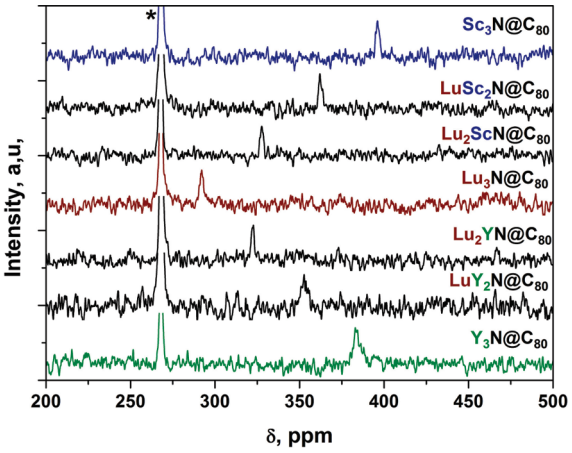

Figure 1. ^{14}N NMR spectra of $Lu_xSc_{3-x}N@C_{80}$ and $Lu_xY_{3-x}N@C_{80}$ ($x = 0 − 3$) in CS_2 at room temperature. An asterisk marks a signal of the molecular nitrogen.

with mixed-metal clusters, a single peak with a half-width of ca. 2 ppm was observed. Somewhat broader peaks were found for $Lu_2YN@C_{80}$ and $Y_3N@C_{80}$, but this is likely due to the shape of the background noise rather than due to the intrinsic broadness of the signals. Thus, our study clearly shows that ^{14}N NMR spectroscopy can be equally useful either for homometallic or for mixed-metal nitride clusterfullerenes. The symmetry breaking imposed by the substitution of metal atoms in homometallic clusters does not lead to a broadening of ^{14}N NMR peaks.

Another important conclusion which follows from the analysis of the experimental spectra is the incremental dependence of the chemical shifts on the composition of the cluster. While the $\delta(^{14}N)$ values for $Sc_3N@C_{80}$, $Y_3N@C_{80}$, and $Lu_3N@C_{80}$ at 396.1, 383.0, and 292.1 ppm agree well with the earlier report of Dorn et al.,[49] the ^{14}N chemical shift in each series of mixed clusterfullerenes is a perfect linear function of x. In particular, ^{14}N chemical shifts in $LuSc_2N@C_{80}$ and $Lu_2ScN@C_{80}$ are 362.0 and 327.6 ppm, respectively, and hence for $Lu_xSc_{3-x}N@C_{80}$ replacement of one Lu atom by one Sc atom results in the $\Delta\delta(^{14}N|Lu\rightarrow Sc)$ shift of 34.6 ppm for any x. Likewise, ^{14}N chemical shifts in $LuY_2N@C_{80}$ and $Lu_2YN@C_{80}$ are 353.0 and 322.0 ppm, respectively, and the $\Delta\delta(^{14}N|Lu\rightarrow Y)$ increment is 30.4 ppm.

Computation of ^{14}N Chemical Shifts. To interpret the results of experimental measurements, we have performed density functional theory (DFT) computations of ^{14}N shielding constants in $Lu_xSc_{3-x}N@C_{80}$ and $Lu_xY_{3-x}N@C_{80}$ and related systems. First, isotropic shielding constants were computed for all $M_xL_{3-x}N@C_{80}$ molecules at the B3LYP level using an individual gauge for localized orbitals (IGLO) approach[51] with Pipek−Mezey molecular orbital (MO) localization algorithm.[52] In these calculations, Gaussian-type IGLO-III and TZVP basis sets were used for nitrogen and carbon atoms, respectively; the def2-TZVP basis set was used for Sc and Y, and the scalar-relativistic SD (28, MWB) effective core potential (removing 28 core electrons) with TZVP-quality basis set was employed for Lu. In the following, this combination of basis sets will be abbreviated as "GTO".

Figure 2 shows the perfect linear correlation between experimental and computed ^{14}N isotropic chemical shifts. Thus, although the slope is only 0.49, the results of computations are

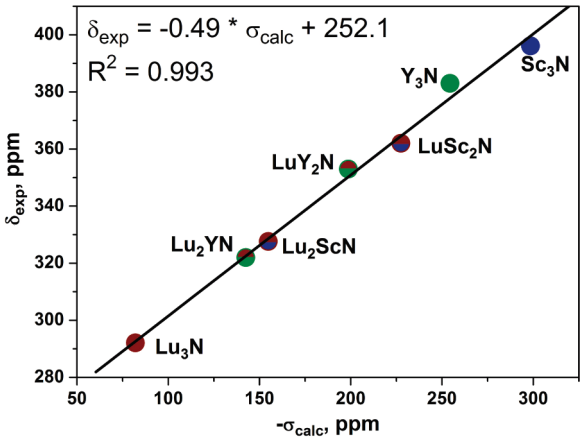

Figure 2. Experimental ^{14}N chemical shifts vs B3LYP/GTO-IGLO computed isotropic shielding constants.

in qualitatively good agreement with experimental data and show that (i) the chemical shifts of $Y_3N@C_{80}$ is much closer to $Sc_3N@C_{80}$, while that of $Lu_3N@C_{80}$ is shielded considerably higher, and (ii) in the mixed clusterfullerenes $Sc_xLu_{3-x}N@C_{80}$ and $Y_xLu_{3-x}N@C_{80}$ the shifts are linear functions of the cluster composition. These facts encouraged us to analyze the different contributions to chemical shifts in more detail. In the view of an additive nature of $\delta(^{14}N)$ values, we limit our analysis in the following to the homometallic clusters Sc_3N, Y_3N, and Lu_3N. Test studies have also shown that the influence of geometrical parameters on ^{14}N chemical shifts is relatively weak. For instance, the use of $Lu_3N@C_{80}$ optimized coordinates for $Y_3N@C_{80}$ resulted in the shift of $\sigma(^{14}N)$ by 17 ppm at the B3LYP/GTO-IGLO level. Likewise, when optimized coordinates of $Sc_3N@C_{80}$ and $Y_3N@C_{80}$ were used for $Lu_3N@C_{80}$, the shifts $\sigma(^{14}N)$ values were −3 and −16 ppm, respectively. Thus, the changes in the ^{14}N chemical shifts in the series of nitride clusterfullerenes cannot be explained by the changes in their geometrical parameters.

Since the metal-nitride cluster formally donates 6 electrons to the carbon cage, it is reasonable to distinguish two contributions to the $\sigma(^{14}N)$ values in $M_3N@C_{80}$. First, the nitrogen nuclei is affected by the interactions with metal atoms in M_3N^{6+} clusters; second, encapsulation of the M_3N^{6+} cluster into the 6-fold charged C_{80}^{6-} cage should also induce the changes in the local magnetic field in the vicinity of the nitrogen atom.

To estimate the influence of the first factor, we have computed ^{14}N chemical shifts in M_3N^{6+} clusters at the same level of theory and with the same atomic coordinates as optimized for $M_3N@C_{80}$ structures. As can be seen in Table 1, in the bare M_3N^{6+} clusters the nitrogen is considerably deshielded in comparison to $M_3N@C_{80}$. Interestingly, the difference between isotropic shielding constants of ^{14}N in Sc_3N^{6+} and Y_3N^{6+} (304 ppm) is more pronounced than the difference between Y_3N^{6+} and Lu_3N^{6+} (192 ppm). Encapsulation of the cluster into the carbon cage dramatically modifies nitrogen shielding constants. In particular, the shielding induced by the encapsulation within the carbon cage, $\Delta\sigma(^{14}N|M_3N^{6+}\rightarrow M_3N@C_{80})$, is as large as 387 ppm for Sc_3N; smaller but still large changes of 128 and 108 ppm are found for Y_3N and Lu_3N, respectively. Nuclear-independent shielding constant in the position of the nitrogen atoms computed for the empty 6-fold charged C_{80}^{6-} cages does not exceed 24 ppm, and hence the changes in the $\sigma(^{14}N)$ values

Table 1. Isotropic $\sigma(^{14}N)$ Values in $M_3N@C_{80}$, $(M\text{-pent})_3N$, and M_3N^{6+} (M = Sc, Y, Lu) Computed at Different Levels of Theory

molecule	method[a]	M = Sc	M = Y	M = Lu
$M_3N@C_{80}$	B3LYP/GTO, IGLO	−299	−254	−82
	B3LYP/GTO, GIAO	−294	−252	−48
	PBE/GTO, IGLO	−288	−238	−79
	PBE/GTO, GIAO	−289	−242	−38
$(M\text{-pent})_3N$	B3LYP/GTO, IGLO	−344	−324	−175
	B3LYP/GTO, GIAO	−344	−323	−153
	PBE/GTO, IGLO	−347	−313	−174
	PBE/GTO, GIAO	−341	−323	−140
	PBE/STO, GIAO	−336	−307	−280
	PBE/STO+SR-ZORA, GIAO	−322	−266	−133
	PBE/STO+SO-ZORA, GIAO	−324	−281	−185
M_3N^{6+}	B3LYP/GTO, IGLO	−686	−382	−190
	B3LYP/GTO, GIAO	−676	−368	−159
	PBE/GTO, IGLO	−662	−366	−187
	PBE/GTO, GIAO	−653	−355	−154
	PBE/STO, GIAO	−627	−354	−296
	PBE/STO+SR-ZORA, GIAO	−605	−295	−122
	PBE/STO+SO-ZORA, GIAO	−606	−305	−161

[a] GTO stands for the following combination of Gaussian-type basis sets: TZVP (C, H), IGLO-III (N), def2-TZVP (Sc, Y), SD-TZVP (Lu); STO stands for Slater-type orbital TZ2P (or ZORA-TZ2P) basis set used in ADF code.

should be presumably ascribed to the redistribution of the electronic density induced by the cluster-cage bond formation. Thus, the analysis shows that the ionic model for $M_3N@C_{80}$ with additive contributions from M_3N^{6+} and C_{80}^{6-} is not appropriate for explanation of the NMR spectra since $nd-\pi$ interactions play a crucial role in determining the nitrogen chemical shift in nitride clusterfullerenes. Importantly, the magnitude of $\Delta\sigma(^{14}N|M_3N^{6+}\rightarrow M_3N@C_{80})$ values are comparable for Y and Lu, while the value for Sc is much larger. This fact agrees well with other spectroscopic as well as electrochemical studies which showed that the cluster-cage interactions in $Y_3N@C_{80}$ and $Lu_3N@C_{80}$ are very similar and more ionic than those in $Sc_3N@C_{80}$, which deviates significantly from other $M_3N@C_{80}$ NCFs.[2,44] On the basis of their results, it can be concluded that the close coincidence of the ^{14}N chemical shifts in $Sc_3N@C_{80}$ and $Y_3N@C_{80}$ results from the interplay of two terms, large deshielding in Sc_3N^{6+}, and large shielding induced by the Sc_3N-cage interactions.

To verify these conclusions, we have also studied the model system in which each metal atom in M_3N cluster is coordinated by pentalene C_8H_6 ("pent" hereafter). One pentalene unit acts as a two-electron acceptor, and hence three pentalenes in $(M\text{-pent})_3N$ can effectively mimic the fullerene cage. Indeed, B3LYP-IGLO computations show that in the $(M\text{-pent})_3N$ systems, ^{14}N shielding constants are close to those in $M_3N@C_{80}$ and exhibit similar trends in that the interaction with the carbon-based π-system induces much larger nitrogen shielding for Sc_3N than for Y_3N and Lu_3N (for all metals, three pentalene units induce somewhat smaller shifts of $\Delta\sigma(^{14}N)$ values than C_{80}). This similarity allows us to use $(M\text{-pent})_3N$ as a model system for a deeper study of the factors affecting the ^{14}N chemical shift.

To summarize, a preliminary analysis of the isotropic shielding constants shows that complete interpretation of the ^{14}N NMR

spectra of $M_xL_{3-x}N@C_{80}$ requires understanding of (i) the reasons of the large variation of $\sigma(^{14}N)$ values in bare M_3N^{6+} clusters and (ii) the factors affecting the changes in nitrogen shielding constants when the clusters are set into interaction with the π-system.

In Ramsey's theory for nuclear magnetic shielding,[50,53] the components of the shielding tensor are evolved as a sum of two terms: (i) diamagnetic term, which is arising from the unperturbed ground-sate wave function, and (ii) paramagnetic term, which describes the currents induced by excitations of the ground-state wave function by the magnetic filed perturbation. For the majority of chemical elements (except for hydrogen), the diamagnetic term is highly transferable (i.e., it is the same in different chemical environments), while the differences in the chemical shifts are mainly due to the variation of the paramagnetic term. For a single-determinant approach (such as DFT), paramagnetic term of the shielding tensor components for nuclei A can be expressed as a double sum over occupied and virtual MOs in a following manner

$$\sigma^{\mathrm{para}}_{\mathrm{A},\alpha\beta} = \frac{2}{c^2}\sum_{k}^{\mathrm{occ}}\sum_{a}^{\mathrm{virt}}\frac{\langle\varphi_k|L_\beta|\varphi_a\rangle\langle\varphi_a|L_{\mathrm{A},\alpha}R_{\mathrm{A}}^{-3}|\varphi_k\rangle}{\Delta E_{k\rightarrow a}} \quad (1)$$

where (α,β) stand for Cartesian directions (x, y, or z), φ_k and φ_a denote occupied and virtual MOs, $L_{\alpha(\beta)}$ is an angular momentum operator in direction $\alpha(\beta)$, $L_{\mathrm{A}.\alpha}$ is the local angular momentum operator acting about the nuclei A, R_{A} is the distance from nuclei A, while $\Delta E_{k\rightarrow a}$ is excitation energy roughly equal to the difference of orbital energies $\varepsilon_a - \varepsilon_k$. The equation is valid for a case of common gauge origin, which is not used in practical computations, while distributed gauge origins modify the equations by introducing additional terms. However, eq 1 can be used to explain the general trends in the computed values. In particular, when canonical MOs are used in the evaluation of shielding constants as in GIAO approach,[54] analysis of contribution from individual excitations from occupied to virtual MOs (occ→virt hereafter) is possible. On the other hand, chemically relevant information can be clearly visualized if the shielding is expressed in terms of contributions from localized or semilocalized MOs such as used in IGLO method.[51] Similar results can be also obtained with natural chemical shielding (NCS) analysis,[55] in which GIAO-computed shielding tensor is expressed in terms of contributions from natural localized molecular orbitals (NLMOs), which are in due turn built from NBO orbitals.[56]

Interpretation of shielding constants in terms of localized and canonical MOs provides a complementary description of the local magnetic phenomena and hence can be even more comprehensive when the two approaches are combined.[57,58] Unfortunately, none of the quantum-chemical codes available to us can give the full analysis of shielding constants using both schemes. Hence, in the following we have combined the information obtained from computations at different levels of theory with different software and unavoidably using different numerical procedures. To ensure that the trends in shielding constants and interpretation of these trends obtained with the help of different codes are universal, first we have compared isotropic shielding constants computed by different density functionals, basis sets, and schemes of shielding tensor computations.

Table 1 compares isotropic shielding constants of $M_3N@C_{80}$, $(M\text{-pent})_3N$, and M_3N^{6+} computed with B3LYP/GTO and PBE/GTO approaches and IGLO as well as GIAO formalisms. First, the data set shows that for Sc and Y, IGLO and GIAO methods give similar results (within 10 ppm) showing that the basis set convergence is almost achieved (note that the IGLO and GIAO values are computed using different quantum chemical codes and hence the difference in internal numerical procedures and parameters can slightly influence the results). For Lu, deviations of IGLO from GIAO schemes are more pronounced but still do not change the qualitative situation. B3LYP and PBE values obtained with the same basis set are also rather similar which shows that the effect of specific density functional form is rather weak and both hybrid and GGA functionals give comparable trends in the computed values when the same basis sets are used.

PBE-GIAO computations were also performed with the full-electron Slater-type orbital TZ2P basis set implemented in ADF package (denoted PBE/STO hereafter). For Sc_3N^{6+}, the PBE/STO value deviates from PBE/GTO analogue by 26 ppm, which is noticeable but not yet crucial, while for Y_3N^{6+} almost the same value is obtained. For Lu_3N^{6+}, nonrelativistic (NR) PBE/STO computations give dramatically different results from PBE/GTO(ECP) values. At this level, $\sigma(^{14}N)$ in Lu_3N^{6+} is −296 ppm, which makes Lu_3N^{6+} much closer to Y_3N^{6+} ($\sigma(^{14}N)$ = −354 ppm) than at the PBE/GTO(ECP) level, at least when compared to Sc_3N^{6+} ($\sigma(^{14}N)$ = −627 ppm). The use of scalar-relativistic (SR) ZORA approximation for Sc_3N^{6+} and Y_3N^{6+} reduces the PBE/STO computed isotropic shielding constant by 22 and 49 ppm, respectively, which shows that for these metals relativistic effects are significant but not yet crucial for the goals of this study. For Lu_3N^{6+}, the effect of SR corrections for the full-electron basis set is much more pronounced: SR-ZORA correction shifts the $\sigma(^{14}N)$ value in Lu_3N^{6+} by as much as 174 ppm. To estimate the further influence of the more rigorous treatment of the relativism, we have also computed $\sigma(^{14}N)$ values using spin−orbital (SO) corrections within ZORA formalism.[59] Here again the relativistic effect for Lu is much more pronounced: while SO corrections are negligible for Sc_3N^{6+} (−1 ppm) and relatively small for Y_3N^{6+} (−10 ppm), a correction of −39 ppm is found for Lu_3N^{6+}. These results show that with the full-electron basis sets, at least scalar-relativistic corrections are necessary for Lu even if only qualitative trends are considered. The values computed with the full-electron STO basis set and SR-ZORA approximation are systematically shifted from the PBE/GTO values (with SR core potential for Lu), but the overall trend is fairly the same. Analogous results were also obtained for $(M\text{-pent})_3N$ systems (Table 1): PBE/GTO-GIAO and NR-PBE/STO-GIAO methods give similar results for Sc and Y but substantially deviate for Lu; ZORA introduces very strong correction for Lu and considerably smaller changes for Sc and Y, while spin−orbit corrections introduce infinitesimal change for Sc and somewhat larger changes for Y and Lu.

To summarize, the $\sigma(^{14}N)$ values listed in Table 1 show that although different methods can give somewhat different results, the trends in $Sc_3N-Y_3N-Lu_3N$ values are always the same (except for nonrelativistic treatment of Lu, which should be avoided), and hence the trends in individual orbital contributions to shielding constants discussed below also have an universal character and will be discussed as such.

Natural Chemical Shielding Analysis. Table 2 shows components of the ^{14}N shielding tensors of M_3N^{6+} in comparison to $(M\text{-pent})_3N$ molecules as computed at the B3LYP-GIAO level and their decomposition into contributions from natural localized molecular orbitals (NLMOs) obtained by NCS analysis (numerical instabilities of the procedure precluded NCS analysis

Table 2. NCS Analysis of B3LYP/GTO-GIAO Computed ^{14}N Shielding Tensors in M_3N^{6+} and $(M\text{-pent})_3N$ (M = Sc, Y, Lu)

NLMO[a]	σ	M_3N^{6+} total	para	dia	$(M\text{-pent})_3N$ total	para	dia	$\Delta\sigma(M_3N^{6+}\rightarrow(M\text{-pent})_3N)$ total
					M = Sc			
1s(N)	σ_{iso}	239	0	239	240	0	240	1
2s(N)	σ_{iso}	32	0	32	31	0	31	−1
$2p_{x(y)}$(N)	σ_{iso}	−398	−410	12	−297	−299	2	101
	$\sigma_{xx(yy)}$	14	−1	13	14	−1	15	0
	$\sigma_{yy(xx)}$	−575	−585	11	−457	−450	−7	118
	σ_{zz}	−633	−646	13	−450	−447	−3	183
$2p_z$(N)	σ_{iso}	−126	−151	25	47	22	25	173
	$\sigma_{xx,yy}$	−197	−228	30	63	33	30	260
	σ_{zz}	15	1	14	15	0	15	0
ΣM(core)	σ_{iso}	−25	−24	−1	−22	−21	−1	3
$\Sigma\pi_{CC}$-d(M)	σ_{iso}				−42	−42	0	
total	$\boldsymbol{\sigma_{iso}}$	**−676**	**−996**	**320**	**−344**	**−639**	**298**	**332**
	$\sigma_{xx(yy)}$	−501	−830	326	−144	−466	320	357
	σ_{zz}	−1025	−1329	306	−744	−1041	297	281
					M = Y			
1s (N)	σ_{iso}	239	0	239	240	0	240	1
2s (N)	σ_{iso}	31	−1	32	33	2	31	2
$2p_{x(y)}$(N)	σ_{iso}	−287	−303	15	−282	−287	5	5
	$\sigma_{xx(yy)}$	13	−2	15	14	−1	15	1
	$\sigma_{yy(xx)}$	−372	−386	14	−416	−415	−1	44
	σ_{zz}	−504	−518	17	−443	−445	2	61
$2p_z$(N)	σ_{iso}	−30	−56	26	41	15	26	71
	$\sigma_{xx,yy}$	−48	−79	32	54	23	31	102
	σ_{zz}	6	−10	16	15	0	15	9
ΣM(core)	σ_{iso}	−36	−33	−3	−41	−39	2	5
$\Sigma\pi_{CC}$-d(M)	σ_{iso}				−32	−32	0	
total	$\boldsymbol{\sigma_{iso}}$	**−368**	**−695**	**326**	**−323**	**−628**	**306**	**42**
	$\sigma_{xx(yy)}$	−153	−495	335	−102	−433	329	51
	σ_{zz}	−796	−1103	312	−766	−1057	291	30
					M = Lu			
1s (N)	σ_{iso}	239	0	239	240	0	240	1
2s (N)	σ_{iso}	32	0	32	31	0	31	−1
$2p_{x(y)}$(N)	σ_{iso}	−220	−231	11	−196	−210	14	24
	$\sigma_{xx(yy)}$	14	−1	15	14	−1	15	0
	$\sigma_{yy(xx)}$	−329	−336	7	−278	−290	12	51
	σ_{zz}	−345	−355	10	−324	−338	−14	21
$2p_z$(N)	σ_{iso}	34	7	27	43	17	26	9
	$\sigma_{xx,yy}$	43	10	33	56	25	31	13
	σ_{zz}	16	0	16	15	0	15	−1
ΣM(core)	σ_{iso}	−27	−25	−2	−22	−21	−1	5
$\Sigma\pi_{CC}$-d(M)	σ_{iso}				−55	−51	−4	
total	$\boldsymbol{\sigma_{iso}}$	**−159**	**−480**	**317**	**−153**	**−475**	**319**	**6**
	$\sigma_{xx(yy)}$	−10	−343	333	29	−313	336	39
	σ_{zz}	−452	−752	300	−516	−818	313	−64

[a] ΣM(core) and $\Sigma\pi_{CC}$-d(M) stand for total contributions from core orbitals of metal atoms and from NL bonding orbitals with dominant π_{CC} contributions with d(M) admixtures (see Figure 3e)

of $M_3N@C_{80}$). The components of the ^{14}N shielding tensor are mostly determined by five NLMOs, all with a presumable contribution from nitrogen AOs. NLMOs of 1s(N) and 2s(N) character contribute 240 and 30 ppm, respectively, to the diamagnetic shielding. This shielding is purely isotropic and perfectly transferable within the whole set of M_3N-based molecules (identical values were found for all studied systems irrespective of the metal or π-ligand). Large variations in ^{14}N shielding constants are caused by three metal−nitrogen bonding NLMOs, each constituting ca. 85−90% of $2p_\alpha$(N) atomic orbital

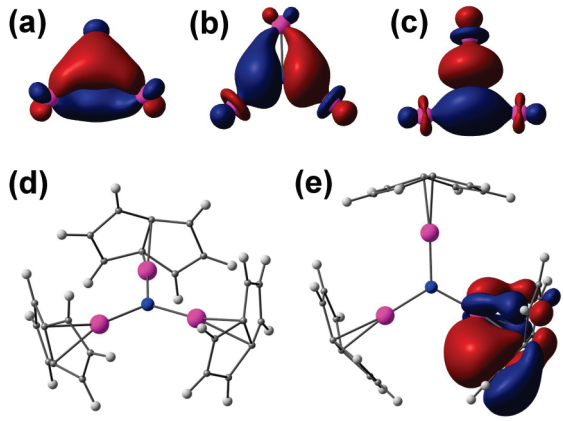

Figure 3. (a−c) Natural localized molecular orbitals (NLMOs) of Sc_3N^{6+} with dominant $2p_{x,y,z}(N)$ contributions (ca. 80%), z axis is perpendicular to the cluster plane; (d) model $(Sc\text{-}pent)_3N$ molecule; (e) an example of π_{CC}-d(M) NLMO in $(Sc\text{-}pent)_3N$ with considerable paramagnetic contribution to $\sigma(^{14}N)$.

(α stands for x, y, or z) and ca. 10−15% of valence nd AOs of corresponding metal atoms. Diamagnetic contributions of these NLMOs exhibit larger variations than those of s(N) counterparts, but their absolute values are rather small. Much more important is the paramagnetic deshielding induced by these NLMOs. Table 2 shows that this term is highly sensitive either to the nature of metal or to the interaction with the π-system and is the reason of the high anisotropy of ^{14}N shielding tensor (the deshielding is much stronger in z direction perpendicular to the M_3N plane). It can be also seen that $2p_{x,y}(N)$-based NLMOs give much higher negative contribution to $\sigma(^{14}N)$ than $2p_z(N)$-based NLMO, and σ_{zz} component is always larger than $\sigma_{xx(yy)}$. At this point, it is instructive to give a more detailed insight into the terms in eq 1. In MO presentation, the action of operator L_α on an orbital can be understood as a rotation of the orbital by 90° around the α-direction (i.e., an action of L_z on p_x AO gives p_y; with this respect p_α paramagnetic contribution to $\sigma_{\alpha\alpha}$ is always vanishing). The first term in the numerator ensures the good overlap of L_α-transformed occupied MO and a virtual MO, while the R_A^{-3} localizes the contribution of occ→virt excitations to the atom of interest. Finally, denominator enhances the weight of the low-energy transitions. In a few words, eq 1 shows that the largest contributions to paramagnetic shielding of ^{14}N nuclei are caused by interactions between occupied and low-energy virtual orbitals with large contributions from the nitrogen atom. It is thus not surprising that NCS analysis shows the dominating role of $2p_\alpha(N)$ AOs in the $\sigma(^{14}N)$.

In addition to the five nitrogen-based NLMOs, noticeable (but not major) contributions to $\sigma(^{14}N)$ are added by two types of NLMOs. A value of −30 ppm is added to the paramagnetic term of $\sigma(^{14}N)$ by the outermost core shells of metal atoms (3s and 3p in Sc, 4s and 4p in Y, etc). These contributions are weakly dependent on the bonding situation and are virtually identical in M_3N^{6+} and $(M\text{-}pent)_3N$. Finally, in $(M\text{-}pent)_3N$ molecules, an additional deshielding is induced by carbon−carbon−metal bonding NLMOs (each MO is constituted from ca. 85−90% π_{CC} and 10−15% nd components). The net contribution of these NLMOs in $\sigma(^{14}N)$ values are −42, −32, and −55 ppm for Sc, Y, and Lu, respectively.

Canonical Orbital Analysis. As the last step of analysis, it is necessary to clarify which unoccupied MOs are responsible for

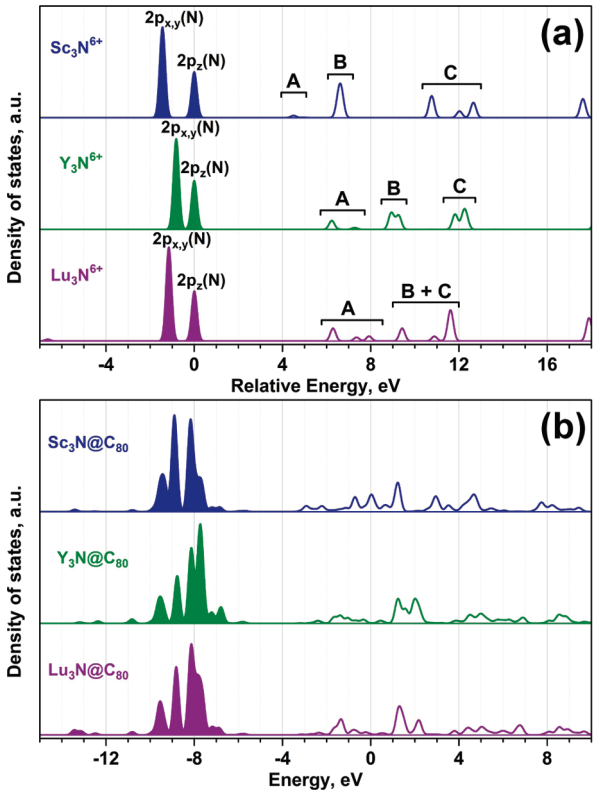

Figure 4. p(N)-projected density of states (B3LYP/GTO level) in (a) M_3N^{6+} and (b) $M_3N@C_{80}$ (M = Sc, Y, Lu). For occupied states, the area under the curves is filled. For the sake of comparison, relative energy scale is used for M_3N^{6+} (the energy of HOMO is set to 0 in each case), while for the $M_3N@C_{80}$ molecules, an actual scale is used (with B3LYP-computed MO energies).

the large local fields induced by $2p_\alpha(N)$→virt excitations. Deconvolution of $\sigma_{para}(^{14}N)$ into individual occ→virt contributions is possible with the use of electron paramagnetic resonance/NMR module of ADF only at the nonrelativistic PBE/(STO-TZ2P) level. Analysis of the MOs shows that the shapes and relative energies of MOs obtained at the B3LYP and PBE levels are sufficiently close to give the same trends in shielding constants, so the results can be discussed here notwithstanding the method of theory used. Figure 4 plots the electronic density of states projected to the $p_{x,z,y}(N)$ AOs (denoted as p(N)-PDOS hereafter; for the sake of comparison to $M_3N@C_{80}$, B3LYP-computed PDOS is plotted). According to their contribution to the paramagnetic shielding of the nitrogen nuclei, the virtual orbitals of Sc_3N^{6+} can be classified into three types (see Figure 4). The lowest energy virtual MOs (within the range of ca. 2−3 eV above LUMO) belong to the type **A**, which is characterized by negative shielding induced by occ$(2p_{x,y}(N))$→virt(**A**) excitations and positive shielding induced by occ$(2p_z(N))$→virt(**A**) excitations, so that the net contribution from occ→virt(**A**) term to the shielding is close to zero. In general, nitrogen contributions to type-**A** MOs are below a few percent, and individual occ→virt excitations induce the (de)shielding of less than 30 ppm. Two virtual MOs constituting the type **B** are the most important for the paramagnetic term. For Sc_3N^{6+}, one of them is a 2-fold degenerate MO with ca. 20% from $2p_{x,y}(N)$, while another one is the MO with 25% of $2p_z(N)$. For Sc_3N^{6+}, occ$(2p_{x,y}(N))$→virt(**B**) term is as large as 2 × −364 ppm, while

dx.doi.org/10.1021/jp204290f |J. Phys. Chem. C 2011, 115, 15257–15265

occ($2p_z$(N))→virt(B) excitations yield the shielding of −200 ppm. Finally, MOs with 3p(N) components constitute type **C**, and occ($2p_{x,y}$(N))→virt(**C**) excitations induce upfield shifts of 2 × 115 ppm. In total, occ→virt excitations in Sc_3N^{6+} yield isotropic deshielding of −727 ppm (−270 ppm are also contributed by occ→occ rotations which appear in GIAO ansatz and have no clear chemical meaning).

The same types of MOs and occ→virt excitations can be distinguished in Y_3N^{6+} and Lu_3N^{6+} clusters; however the differences in electronic properties of the metals result in large deviations of the shielding. Larger populations of 2p(N) AOs (larger negative charge on nitrogen) in Y_3N^{6+} as compared to that in Sc_3N^{6+} result in smaller 2p(N) contributions to the virtual MOs of the type **B**; besides, the relative energies of these MOs are higher. As a result, the occ($2p_{x,y}$(N))→virt(**B**) and occ($2p_z$(N))→virt(**B**) terms in Y_3N^{6+} are reduced to 2 × −203 and −102 ppm, respectively. The occ($2p_{x,y}$(N))→virt(**C**) term is also reduced to only 2 × 30 ppm, and the net isotropic deshielding of −473 ppm induced by occ→virt excitations is found in Y_3N^{6+} (occ→occ term yields −227 ppm).

Thus, once the dominating role of occ($2p_\alpha$(N))→virt(**B,C**) excitations is revealed, the differences in $\sigma(^{14}N)$ values of Sc_3N^{6+} and Y_3N^{6+} can be easily explained by a simple analysis of p(N)-PDOS. Interpretation of the $\sigma(^{14}N)$ values in Lu_3N^{6+} is now also straightforward. As outlined above, nonrelativistic computations predict that $\sigma(^{14}N)$ in Lu_3N^{6+} is close to that in Y_3N^{6+}. Likewise, their p(N)-PDOS distributions are also rather similar. Relativistic effect results in the shift of type-**B** MOs to higher energies so that they are found in the same energy range with type-**C** MOs; at the same time, $2p_{x,y}$(N)-based MOs are shifted to lower energies with respect to $2p_z$(N)-based MO, and as a result, paramagnetic deshielding in Lu_3N^{6+} is reduced due to the increase of the denominator in eq 1. Thus, it can be concluded that the large difference in $\sigma(^{14}N)$ values between Y_3N^{6+} and Lu_3N^{6+} is mostly relativistic in nature.

The changes in nitrogen shielding tensor induced by interactions with the π-system can be easily explained by the changes of p(N)-PDOS. It should be noted that in M_3N^{6+} systems, $2p_\alpha$(N)-based NLMOs and canonical MOs have virtually identical shapes and hence NLMO and canonical MO analyses operate with virtually the same MOs (the only difference is that canonical MOs are symmetrized). In more complex molecules with π-ligands, NLMOs and canonical MOs are substantially different because of admixing of carbon-derived AOs. Yet, it can be clearly seen in Figure 4 that canonical MOs with large contributions from $2p_\alpha$(N) AOs in $M_3N@C_{80}$ are clustering in rather narrow energy range and hence p(N)-PDOS distribution is still comparable to that of M_3N^{6+}. As we have shown above, the contribution of any occ→virt excitation to the shielding tensor is determined solely by the p_α(N) components in the involved MOs, and therefore all arguments derived for M_3N^{6+} apply to the more complex systems as well. Dramatic decrease of the $\sigma^{para}(^{14}N)$ values in $Sc_3N@C_{80}$ in comparison to Sc_3N^{6+} correlates well with the considerable high-energy shift and smearing of the type-**B** peaks in the unfilled p(N)-PDOS; at the same time, type-**C** peaks are found at the same energy (with respect to occupied MOs). In $Y_3N@C_{80}$ and $Lu_3N@C_{80}$, the differences in p(N)-PDOS induced by the interaction with carbon cage are much smaller so that the relative energies of the main components are more or less the same, and the only difference is the smearing of the distribution. As a result, changes in the shielding induced by the interaction with the π-system are much smaller for these metals.

CONCLUSIONS

^{14}N NMR spectroscopy was shown to be a powerful tool in the studies of both homometal- and mixed-metal nitride clusterfullerenes. ^{14}N chemical shifts were found to be sensitive to the cluster composition. In the mixed-metal nitride clusterfullerenes, ^{14}N chemical shift is shown to be a linear function of the cluster composition. Thus, the study of all three structural "shells" in nitride clusterfullerenes, namely, a carbon cage, metal atoms, and a central nitrogen atom, is now possible by NMR spectroscopy.

DFT computations were shown to provide good correlations with the experimental values which encouraged us to provide a detailed analysis of the shielding tensors in terms of Ramsey theory. We have shown that ^{14}N chemical shifts in $M_3N@C_{80}$ and related systems are solely determined by nitrogen-localized orbitals. In particular, the variation of ^{14}N chemical shifts in different compounds can be traced back to the $p_{x,y,z}$ atomic orbitals of nitrogen and their contribution to the paramagnetic shielding. As a result, the changes in the nitrogen shielding can be clarified by the simple analysis of the p(N) projected density of states and its variation in different chemical environments.

EXPERIMENTAL SECTION

Synthesis and HPLC separation of mixed-metal nitride clusterfullerenes $Lu_xSc_{3-x}N@C_{80}$ and $Lu_xY_{3-x}N@C_{80}$ (x = 0−3) was reported earlier.[14,47] ^{14}N NMR spectroscopic study was performed at 36,14 MHz in a multiprobe head PH 1152Z of an Avance II 500 spectrometer (Bruker) at room temperature (288 K) in carbon disulfide solutions with d_6-acetone as an external lock in a coaxial tube and an aqueous NH_4^+ as a reference.

Details of Computations. Optimization of the molecular structure of all species reported in this work was performed using PBE functional[60] and TZ2P-quality basis set (full-electron {6,3,2}/(11s,6p,2d) for C and N atoms and SBK-type effective core potential for Sc, Y, and Lu atoms with {5,5,4}/(9s,9p,8d) valence part) implemented in the PRIRODA package.[61,62] The code employed expansion of the electron density in an auxiliary basis set to accelerate evaluation of the Coulomb and exchange-correlation terms.[61] For $\sigma(^{14}N)$ computations, M−N bonds in PBE/TZ2P optimized $(M\text{-pent})_3N$ molecular structures were modified to be equal to those of $M_3N@C_{80}$ molecules. Coordinates for M_3N^{6+} clusters were taken from optimized $M_3N@C_{80}$ clusterfullerenes without further optimization.

PBE-IGLO and B3LYP-IGLO computations with Pipek-Mezey MO localization algorithm[52] were performed using ORCA package.[63] IGLO-III[51] {51111111/211111/11} and TZVP[64] {62111/411/1} basis sets were used for nitrogen and carbon atoms, respectively. For Sc and Y metal atoms, we used full-electron def2-TZVP[65] {842111/6311/4111/1} and {842111 11/641111/51111/1} basis sets, respectively, while scalar-relativistic SD (28, MWB) effective core potential[66,67] (removing 28 core electrons) with TZVP[68] {5111111111/61111111/61111/5111/1} basis set for valence and semicore electrons were employed for Lu. In B3LYP calculations, RIJCOSX algorithm[69,70] was used to accelerate evaluation of exact exchange terms.

The same basis sets as in IGLO computations were also employed in PBE-GIAO and B3LYP-GIAO computations performed with the use Gaussian 09-A.02 package.[71] This package was also used for NCS analysis.[55]

PBE-GIAO computations[59,72,73] and analysis of chemical shifts in terms of canonical MOs with full electron basis sets

were also performed using ADF 2010.02[74,75] and Slater-type TZ2P basis set (or its ZORA variant for relativistic calculations).[76]

AUTHOR INFORMATION

Corresponding Author

*E-mail: a.popov@ifw-dresden.de (A.A.P.); l.dunsch@ifw-dresden.de (L.D.).

Present Addresses

[#]Hefei National Laboratory for Physical Sciences at Microscale, Department of Materials Science and Engineering, University of Science and Technology of China.

ACKNOWLEDGMENT

The authors acknowledge financial support by AvH and DFG (to A.A.P.), Erasmus Mundus programme External Co-operation (EM ECW-L04 TUD 08-11, to S.M.), and World Class University program sponsored by the South Korean Ministry of Education, Science, and Technology Program, (Project No. R31-2008-000-10100-0 to G. C.). Computational Center in Moscow State University is acknowledged for computer time on "Chebyshev SKIF-MSU" supercomputer; the authors also thank the Center for Information Services and High Performance Computing (ZIH) of TU Dresden for computational time on its clusters. Technical assistance of U. Nitzsche with local computer resources at IFW is highly appreciated.

REFERENCES

(1) Dunsch, L.; Yang, S. *Small* **2007**, *3* (8), 1298–1320.

(2) Chaur, M. N.; Melin, F.; Ortiz, A. L.; Echegoyen, L. *Angew. Chem., Int. Ed.* **2009**, *48*, 7514–7538.

(3) Dunsch, L.; Yang, S. F. *Phys. Chem. Chem. Phys.* **2007**, *9* (24), 3067–3081.

(4) Popov, A. A. *J. Comput. Theor. Nanosci.* **2009**, *6* (2), 292–317.

(5) Valencia, R.; Rodriguez-Fortea, A.; Clotet, A.; de Graaf, C.; Chaur, M. N.; Echegoyen, L.; Poblet, J. M. *Chem.—Eur. J.* **2009**, *15* (41), 10997–11009.

(6) Popov, A. A.; Dunsch, L. *J. Phys. Chem. Lett.* **2011**, *2* (7), 786–794.

(7) Yamada, M.; Wakahara, T.; Lian, Y.; Tsuchiya, T.; Akasaka, T.; Waelchli, M.; Mizorogi, N.; Nagase, S.; Kadish, K. M. *J. Am. Chem. Soc.* **2006**, *128* (5), 1400–1401.

(8) Takano, Y.; Aoyagi, M.; Yamada, M.; Nikawa, H.; Slanina, Z.; Mizorogi, N.; Ishitsuka, M. O.; Tsuchiya, T.; Maeda, Y.; Akasaka, T.; Kato, T.; Nagase, S. *J. Am. Chem. Soc.* **2009**, *131*, 9340–9346.

(9) Yamada, M.; Someya, C.; Wakahara, T.; Tsuchiya, T.; Maeda, Y.; Akasaka, T.; Yoza, K.; Horn, E.; Liu, M. T. H.; Mizorogi, N.; Nagase, S. *J. Am. Chem. Soc.* **2008**, *130*, 1171–1176.

(10) Yamada, M.; Wakahara, T.; Tsuchiya, T.; Maeda, Y.; Akasaka, T.; Mizorogi, N.; Nagase, S. *J. Phys. Chem. A* **2008**, *112*, 7627–7631.

(11) Zhang, L.; Popov, A. A.; Yang, S.; Klod, S.; Rapta, P.; Dunsch, L. *Phys. Chem. Chem. Phys.* **2010**, *12*, 7840–7847.

(12) Wang, X. L.; Zuo, T. M.; Olmstead, M. M.; Duchamp, J. C.; Glass, T. E.; Cromer, F.; Balch, A. L.; Dorn, H. C. *J. Am. Chem. Soc.* **2006**, *128* (27), 8884–8889.

(13) Klod, S.; Zhang, L.; Dunsch, L. *J. Phys. Chem. C* **2010**, *114* (18), 8264–8267.

(14) Yang, S.; Popov, A. A.; Dunsch, L. *Angew. Chem. Int. Edit. Engl.* **2008**, *47*, 8196–8200.

(15) Alvarez, L.; Pichler, T.; Georgi, P.; Schwieger, T.; Peisert, H.; Dunsch, L.; Hu, Z.; Knupfer, M.; Fink, J.; Bressler, P.; Mast, M.; Golden, M. S. *Phys. Rev. B* **2002**, *66* (3), 035107.

(16) Pichler, T.; Golden, M. S.; Knupfer, M.; Fink, J.; Kirbach, U.; Kuran, P.; Dunsch, L. *Phys. Rev. Lett.* **1997**, *79* (16), 3026–3029.

(17) Krause, M.; Liu, X. J.; Wong, J.; Pichler, T.; Knupfer, M.; Dunsch, L. *J. Phys. Chem. A* **2005**, *109* (32), 7088–7093.

(18) Shiozawa, H.; Rauf, H.; Pichler, T.; Grimm, D.; Liu, X.; Knupfer, M.; Kalbac, M.; Yang, S.; Dunsch, L.; Buchner, B.; Batchelor, D. *Phys. Rev. B* **2005**, *72* (19), 5.

(19) Weaver, J. H.; Chai, Y.; Kroll, G. H.; Jin, C.; Ohno, T. R.; Haufler, R. E.; Guo, T.; Alford, J. M.; Conceicao, J.; Chibante, L. P. F.; Jain, A.; Palmer, G.; Smalley, R. E. *Chem. Phys. Lett.* **1992**, *190* (5), 460–464.

(20) Shinohara, H. *Rep. Prog. Phys.* **2000**, *63* (6), 843–892.

(21) Rahmer, J.; Dunsch, L.; Dorn, H.; Mende, J.; Mehring, M. *Magn. Reson. Chem.* **2005**, *43*, S192–S198.

(22) Jakes, P.; Dinse, K. P. *J. Am. Chem. Soc.* **2001**, *123* (36), 8854–8855.

(23) Rapta, P.; Popov, A. A.; Yang, S. F.; Dunsch, L. *J. Phys. Chem. A* **2008**, *112*, 5858–5865.

(24) Popov, A. A.; Shustova, N. B.; Svitova, A. L.; Mackey, M. A.; Coumbe, C. E.; Phillips, J. P.; Stevenson, S.; Strauss, S. H.; Boltalina, O. V.; Dunsch, L. *Chem.—Eur. J.* **2010**, *16* (16), 4721–4724.

(25) Shustova, N. B.; Peryshkov, D. V.; Kuvychko, I. V.; Chen, Y.-S.; Mackey, M. A.; Coumbe, C. E.; Heaps, D. T.; Confait, B. S.; Heine, T.; Phillips, J. P.; Stevenson, S.; Dunsch, L.; Popov, A. A.; Strauss, S. H.; Boltalina, O. V. *J. Am. Chem. Soc.* **2011**, *133* (8), 2672–2690.

(26) Hoinkis, M.; Yannoni, C. S.; Bethune, D. S.; Salem, J. R.; Johnson, R. D.; Crowder, M. S.; Devries, M. S. *Chem. Phys. Lett.* **1992**, *198* (5), 461–465.

(27) Misochko, E. Y.; Akimov, A. V.; Belov, V. A.; Tyurin, D. A.; Bubnov, V. P.; Kareev, I. E.; Yagubskii, E. B. *Phys. Chem. Chem. Phys.* **2010**, *12* (31), 8863–8869.

(28) Echegoyen, L.; Chancellor, C. J.; Cardona, C. M.; Elliott, B.; Rivera, J.; Olmstead, M. M.; Balch, A. L. *Chem. Commun.* **2006**, *25*, 2653–2655.

(29) Zuo, T.; Xu, L.; Beavers, C. M.; Olmstead, M. M.; Fu, W.; Crawford, T. D.; Balch, A. L.; Dorn, H. C. *J. Am. Chem. Soc.* **2008**, *130* (39), 12992–12997.

(30) Suzuki, T.; Maruyama, Y.; Kato, T.; Akasaka, T.; Kobayashi, K.; Nagase, S.; Yamamoto, K.; Funasaka, H.; Takahashi, T. *J. Am. Chem. Soc.* **1995**, *117* (37), 9606–9607.

(31) Akasaka, T.; Kato, T.; Nagase, S.; Kobayashi, K.; Yamamoto, K.; Funasaka, H.; Takahashi, T. *Tetrahedron* **1996**, *52* (14), 5015–5020.

(32) Yamada, M.; Okamura, M.; Sato, S.; Someya, C. I.; Mizorogi, N.; Tsuchiya, T.; Akasaka, T.; Kato, T.; Nagase, S. *Chem.—Eur. J.* **2009**, *15* (40), 10533–10542.

(33) Dinse, K. P.; Kato, T. Multi-Frequency EPR Study of Metallo-Endofullerenes. In *Novel NMR and EPR Techniques, Lecture Notes Phys.*; Dolinšek, J.; Vilfan, M.; Žumer, S., Eds.; Springer: Berlin Heidelberg, 2006; pp 185—207.

(34) Kato, T. *J. Mol. Struct.* **2007**, *838* (1—3), 84–88.

(35) Fu, W.; Xu, L.; Azurmendi, H.; Ge, J.; Fuhrer, T.; Zuo, T.; Reid, J.; Shu, C.; Harich, K.; Dorn, H. C. *J. Am. Chem. Soc.* **2009**, *131* (33), 11762–11769.

(36) Miyake, Y.; Suzuki, S.; Kojima, Y.; Kikuchi, K.; Kobayashi, K.; Nagase, S.; Kainosho, M.; Achiba, Y.; Maniwa, Y.; Fisher, K. *J. Phys. Chem.* **1996**, *100*, 9579–9581.

(37) Kurihara, H.; Lu, X.; Iiduka, Y.; Mizorogi, N.; Slanina, Z.; Tsuchiya, T.; Akasaka, T.; Nagase, S. *J. Am. Chem. Soc.* **2011**, *133* (8), 2382–2385.

(38) Stevenson, S.; Rice, G.; Glass, T.; Harich, K.; Cromer, F.; Jordan, M. R.; Craft, J.; Hadju, E.; Bible, R.; Olmstead, M. M.; Maitra, K.; Fisher, A. J.; Balch, A. L.; Dorn, H. C. *Nature* **1999**, *401* (6748), 55–57.

(39) Akasaka, T.; Nagase, S.; Kobayashi, K.; Walchli, M.; Yamamoto, K.; Funasaka, H.; Kako, M.; Hoshino, T.; Erata, T. *Angew. Chem., Int. Ed. Engl.* **1997**, *36* (15), 1643–1645.

(40) Wang, T.-S.; Feng, L.; Wu, J.-Y.; Xu, W.; Xiang, J.-F.; Tan, K.; Ma, Y.-H.; Zheng, J.-P.; Jiang, L.; Lu, X.; Shu, C.-Y.; Wang, C.-R. *J. Am. Chem. Soc.* **2010**, *132* (46), 16362–16364.

(41) Dunsch, L.; Yang, S.; Zhang, L.; Svitova, A.; Oswald, S.; Popov, A. A. *J. Am. Chem. Soc.* **2010**, *132* (15), 5413–5421.
(42) Krause, M.; Kuzmany, H.; Georgi, P.; Dunsch, L.; Vietze, K.; Seifert, G. *J. Chem. Phys.* **2001**, *115* (14), 6596–6605.
(43) Krause, M.; Popov, A.; Dunsch, L. *ChemPhysChem* **2006**, *7* (8), 1734–1740.
(44) Yang, S. F.; Troyanov, S. I.; Popov, A. A.; Krause, M.; Dunsch, L. *J. Am. Chem. Soc.* **2006**, *128* (51), 16733–16739.
(45) Yang, S. F.; Kalbac, M.; Popov, A.; Dunsch, L. *ChemPhysChem* **2006**, *7* (9), 1990–1995.
(46) Yang, S. F.; Popov, A. A.; Kalbac, M.; Dunsch, L. *Chem.—Eur. J.* **2008**, *14* (7), 2084–2092.
(47) Yang, S.; Popov, A. A.; Chen, C.; Dunsch, L. *J. Phys. Chem. C* **2009**, *113* (18), 7616–7623.
(48) Yang, S. F.; Popov, A. A.; Dunsch, L. *Chem. Commun.* **2008**, 2885–2887.
(49) Fu, W.; Wang, X.; Azuremendi, H.; Zhang, J.; Dorn, H. C. *Chem. Commun.* **2011**, *47* (13), 3858–3860.
(50) Ramsey, N. F. *Phys. Rev.* **1950**, *78* (6), 699–703.
(51) Kutzelnigg, W.; Fleischer, U.; Schindler, S. The IGLO-Method: Ab Initio Calculation and Interpretation of NMR Chemical Shifts and Magnetic Susceptibilities. In *NMR Basic Principles and Progress*; Springer Verlag: Berlin/Heidelberg, 1991; pp 165—262.
(52) Pipek, J.; Mezey, P. G. *J. Chem. Phys.* **1989**, *90* (9), 4916–4926.
(53) Kaupp, M.; Buhl, M.; Malkin, V. G. *Calculation of NMR and EPR Parameters. Theory and Applications*; WILEY-VCH Verlag GmbH & Co. KGaA: Weinheim, 2004.
(54) Wolinski, K.; Hinton, J. F.; Pulay, P. *J. Am. Chem. Soc.* **1990**, *112* (23), 8251–8260.
(55) Bohmann, J. A.; Weinhold, F.; Farrar, T. C. *J. Chem. Phys.* **1997**, *107* (4), 1173–1184.
(56) Reed, A. E.; Weinhold, F. *J. Chem. Phys.* **1985**, *83* (4), 1736–1740.
(57) Kaupp, M. *Chem.—Eur. J.* **1998**, *4* (9), 1678–1686.
(58) Kaupp, M. *Chem.—Eur. J.* **1998**, *4* (10), 2059–2071.
(59) Wolff, S. K.; Ziegler, T. *J. Chem. Phys.* **1998**, *109* (3), 895–905.
(60) Perdew, J. P.; Burke, K.; Ernzerhof, M. *Phys. Rev. Lett.* **1996**, *77* (18), 3865–3868.
(61) Laikov, D. N. *Chem. Phys. Lett.* **1997**, *281*, 151–156.
(62) Laikov, D. N.; Ustynyuk, Y. A. *Russ. Chem. Bull., Int. Ed.* **2004**, *54* (3), 820–826.
(63) Neese, F. *ORCA, an ab initio, density functional and semiempirical program package, Version 2.7*; Institute for physical and theoretical chemistry: Bonn, 2009.
(64) Schaefer, A.; Horn, H.; Ahlrichs, R. *J. Chem. Phys.* **1992**, *97* (4), 2571–2577.
(65) Weigend, F.; Ahlrichs, R. *Phys. Chem. Chem. Phys.* **2005**, *7* (18), 3297–3305.
(66) Cao, X.; Dolg, M. *J. Chem. Phys.* **2001**, *115* (16), 7348–7355.
(67) Cao, X.; Dolg, M. *THEOCHEM* **2002**, *581*, 139–147.
(68) Eichkorn, K.; Weigend, F.; Treutler, O.; Ahlrichs, R. *Theor. Chem. Acc.* **1997**, *97* (1—4), 119–124.
(69) Neese, F.; Wennmohs, F.; Hansen, A.; Becker, U. *Chem. Phys.* **2009**, *356* (1—3), 98–109.
(70) Neese, F. *J. Comput. Chem.* **2003**, *24* (14), 1740–1747.
(71) Frisch, M. J.; Trucks, G. W.; Schlegel, H. B.; Scuseria, G. E.; Robb, M. A.; Cheeseman, J. R.; Scalmani, G.; Barone, V.; Mennucci, B.; Petersson, G. A.; Nakatsuji, H.; Caricato, M.; Li, X.; Hratchian, H. P.; Izmaylov, A. F.; Bloino, J.; Zheng, G.; Sonnenberg, J. L.; Hada, M.; Ehara, M.; Toyota, K.; Fukuda, R.; Hasegawa, J.; Ishida, M.; Nakajima, T.; Honda, Y.; Kitao, O.; Nakai, H.; Vreven, T.; Montgomery, Jr., J. A.; Peralta, J. E.; Ogliaro, F.; Bearpark, M.; Heyd, J. J.; Brothers, E.; Kudin, K. N.; Staroverov, V. N.; Kobayashi, R.; Normand, J.; Raghavachari, K.; Rendell, A.; Burant, J. C.; Iyengar, S. S.; Tomasi, J.; Cossi, M.; Rega, N.; Millam, N. J.; Klene, M.; Knox, J. E.; Cross, J. B.; Bakken, V.; Adamo, C.; Jaramillo, J.; Gomperts, R.; Stratmann, R. E.; Yazyev, O.; Austin, A. J.; Cammi, R.; Pomelli, C.; Ochterski, J. W.; Martin, R. L.; Morokuma, K.; Zakrzewski, V. G.; Voth, G. A.; Salvador, P.; Dannenberg, J. J.; Dapprich, S.; Daniels, A. D.; Farkas, Ö; Foresman, J. B.; Ortiz, J. V.; Cioslowski, J.; Fox, D. J. *Gaussian 09*, revision A.02; Gaussian, Inc.: Wallingford, CT, 2009.
(72) Schreckenbach, G.; Ziegler, T. *J. Phys. Chem.* **1995**, *99* (2), 606–611.
(73) Wolff, S. K.; Ziegler, T.; Van Lenthe, E.; Baerends, E. J. *AIP* **1999**, *110*, 7689–7698.
(74) *ADF2010, SCM, Theoretical Chemistry*, Vrije Universiteit, Amsterdam, The Netherlands, http://www.scm.com.
(75) te Velde, G.; Bickelhaupt, F. M.; Baerends, E. J.; Fonseca Guerra, C.; van Gisbergen, S. J. A.; Snijders, J. G.; Ziegler, T. *J. Comput. Chem.* **2001**, *22* (9), 931–967.
(76) Van Lenthe, E.; Baerends, E. J. *J. Comput. Chem.* **2003**, *24* (9), 1142–1156.